AIAA JOURNAL
Vol. 50, No. 11, November 2012

Active Control of Flow-Induced Acoustic Resonance Through Surface Perturbation

Z. B. Lu* and L. Cheng†
Hong Kong Polytechnic University, Kowloon, Hong Kong, People's Republic of China

DOI: 10.2514/1.J051748

A surface perturbation technique was applied to control the flow-induced acoustic resonance inside downstream cavities. The technique made use of piezoceramic actuators embedded on the surface of an upstream test model in a crossflow to generate a controllable motion to alter vortex formation, as well as the subsequent acoustic resonance. Experiments were conducted using various configurations. It was observed that the flow-induced acoustic resonance could be effectively reduced after applying a surface perturbation technique. This was caused not only by an impairment of the vortex-shedding strength but also by a shift in the shedding frequency resulting from the control action. The vortex-strength abatement mechanism was discussed, and the estimation of the frequency-shift phenomenon as well as its effect on the impairment of acoustic resonance was experimentally assessed.

Nomenclature

B	=	width of downstream cavity
c	=	sound speed
d	=	height of duct
d_p	=	displacement of vibration plate
E_u	=	power spectra density
f'_a	=	first acoustic resonance frequency of downstream cavity
f_p	=	control frequency
f_s	=	vortex-shedding frequency
f_{sp}	=	perturbed shedding frequency
h	=	height of test model
L	=	depth of downstream cavity
Re	=	Reynolds number
SPL_{m2}, SPL_{m1}	=	sound pressure levels measured at microphone 2 and microphone 1, respectively
S_t	=	Strouhal number
U_{cr}	=	critical flow velocity at resonance
U_∞	=	freestream flow velocity
V_p	=	control voltage
w	=	width of the test model
Δf_{sp}	=	reduction of shedding frequency
δ	=	thickness of the boundary layer
$\phi_{u_1u_2}$	=	spectral phase

I. Introduction

BLUFF bodies are widely used in many branches of engineering, such as aeronautics and mechanical, chemical, and civil engineering. Reaching a certain flow speed, the periodic vortex shedding occurs in the wake of a bluff body placed in a crossflow, with an oscillatory pressure field around the body generating the structural vibration at the vortex-shedding frequency. Meanwhile, the shed vortices cause strong aerodynamic noise downstream of the bluff body in the flowfield. Although a complete theoretical description of the problem of vortex shedding is still not available, tireless effort has been spent on understanding the vortex-shedding process and on developing ways for its mitigation. Gerrard [1] gave an extremely useful physical description of the mechanics of the vortex formation. A key factor in the formation of a vortex street is the interaction between two separating shear layers. It was postulated that a vortex continues to grow, fed by circulation from its connected shear layer, until it is strong enough to draw the opposing shear layer across the near wake. Both experimental [2] and numerical studies [3] have shown that the shedding from both sides of the bluff body were out of phase and locked to a single frequency.

Extensive work has been carried out in the field of flow-induced vibration control during the last few decades. Flow-induced vibrations can be controlled using either passive or active means [4]. Passive techniques require no energy input, exemplified by surface modifications with roughness [5], splitter plates [6,7], detached plates [8,9], and small secondary control cylinders [10]. Active control methods, however, require energy input via actuators to bring about desirable changes in the shear flow and subsequently alter the flow system. One of the key points to ensuring an effective control is using actuators that can create significant effects on the physical parameters to be controlled. Depending on whether feedback signals are used in the control process, active control can be further divided into open- and closed-loop controls. Typical open-loop control examples include rotary, streamwise, and transverse oscillations of a bluff body and inflow oscillation [11–14]. As typical closed-loop control examples, Berger [15] introduced the single-sensor feedback control by actuating a bimorph cylinder with the signals from a hot-wire sensor located in the wake; Huang and Weaver [16] used the fluctuating acoustic pressure inside a cavity as feedback signals to drive the loudspeakers at the entrance of the tunnel. Cattafesta et al. [17–19] used an oscillating flap hinged near a cavity leading edge to disturb the shear layer separation, with feedback signals taken from the fluctuating acoustic pressure measured by a microphone within the cavity. Cheng et al. [20] used a novel perturbation technique to control the flow-induced vibration, leading to a simultaneous reduction in both flowfield and structural vibration. In the last case, the essence of the technique was to generate a controllable transverse motion over a structural surface using embedded piezoceramic actuators to alter the fluid–structure interactions. The perturbed action to flow was generated by an advanced piezoceramic thin layer composite unimorph driver and sensor (THUNDER) actuator [21] that could provide an appreciable displacement with an acceptable load-bearing capacity. This led to a series of works by Zhang et al. [22–25], who experimentally studied the fluid-structure interaction by using the proposed perturbation technique. It was demonstrated that the actively controlled perturbation could successfully alter the interactions between the synchronizing bluff-body motion and the vortex shedding. Subsequently, both vortex shedding and the flow-induced structural vibration could be simultaneously impaired.

Received 17 November 2011; revision received 18 April 2012; accepted for publication 18 May 2012.

*Ph.D. Student, Department of Mechanical Engineering.
†Chair Professor, Department of Mechanical Engineering.

As a continuation of the previous work, Zhang et al. [26] further investigated the control of the flow-induced acoustic resonance in a duct system comprising an upstream structure as a vortex generator and a downstream acoustic cavity using an open-loop control scheme. A similar arrangement in terms of installation of piezoelectric actuators was adopted. Experiments targeted the occurrence of acoustic resonance when the vortex-shedding frequency coincided with the first acoustic resonance of the downstream cavities. Results pointed to a reduction in the sound pressure level (SPL) inside the resonant cavity, amounting to 8.2 dB, due to the piezo-driven actuation. Apart from the apparent performance of the control, however, the underlying physical mechanism behind the control action still remained unknown. The sound reduction was interpreted as a direct consequence of the vortex-strength impairment, the reason behind which could not be explained either.

The present paper reports an experimental study on the control of flow-induced acoustic resonance based on the perturbation technique. The primary objective is to provide a comprehensive assessment of the efficiency of the technique using an improved actuator configuration and, more importantly, to provide experimental evidence to explain how the perturbation technique attenuates flow-induced sound. In addition to the impaired vortex strength, it was demonstrated that the effective reduction of the acoustic resonance also originated from a perturbation-induced shedding frequency shift, which could be predicted using a simple formula proposed in this paper.

II. Experimental Condition

Experiments were carried out in a closed-circuit acoustic wind tunnel, as schematically shown in Fig. 1. Characteristics of the test facility have been reported previously [26]. Basically, it has a 1.82-m-long square test section of 0.1×0.1 m with a parabolic contraction at the inlet to improve the uniformity of the flow velocity profile and reduce the boundary-layer thickness. A flat-walled diffuser, with a half angle of 14 deg, was used downstream of the working section to increase the pressure recovery. The maximum flow velocity was 50 m/s, with a turbulence intensity of less than 0.1% in the upstream section. The background noise of the tunnel was low since the motor and fan noises were mostly absorbed by an acoustic duct lining.

A so-called test model was installed in the duct, located at 370 mm downstream of the exit plane of the tunnel contraction. It was rigidly fixed on both side walls of the test section and served as a vortex generator with an angle of attack of zero. Two identical cavities with square cross sections were located downstream of the duct, symmetrical to the streamwise flow line. The test model and the cavity dimension, as well as the flow speed, were set so that acoustic resonance took place inside the cavity at the shedding frequency.

A detailed design of the test model and the embodiment of the actuators are shown in Fig. 2. The test model had a semicircular leading edge, a height of $h = 11$ mm, and a width (chord) of $w = 23$ mm. This configuration was determined after a number of tests were conducted using several test models having different widths to ensure that the noise generated by the vortex shedding behind the test model was strong enough. Two curved THUNDER piezoceramic actuators, with a length of 63 mm and a width of 14 mm, were embedded in a slot 16 mm wide and 7 mm deep on the top side of the test model. The actuator was installed with respect to the central axis of the vibration plate, leaving 1 mm at each side, as shown in Fig. 2. The actuators were installed in a cantilever manner to create a maximum perturbation displacement in the transverse y direction and, thus, better control performance. A thin plastic plate 1.2 mm thick was mounted flush with the upper surface of the test model. This thin plate, connected with the cantilevered end of the actuators by using double-sided tape, is referred to as a "vibration plate," providing the perturbation to flow for control purposes. The double-sided tape not only ensured a good connection between the vibration plate and the THUNDER actuators but also provided the flexibility in the installation. The final installation allowed the surface of the vibration plate to be flush with that of the test model before actuation was applied. Driven by the actuators, this vibration plate would oscillate to create a spanwise uniform transverse vibration along the plate surface, as confirmed by the measurement of velocity over the plate using a scanning laser vibrometer.

The entire test configuration together with the measurement system is shown in Fig. 3. The depth (L) and width (B) of the two side cavities were 487 and 70 mm, respectively. The first acoustic resonance frequency of the cavity (f'_a) was approximately estimated by using $f'_a = c/2(2L + d) \approx 161.3$ Hz [27], where c was the speed of sound and d was the height of the duct. The corresponding critical flow velocity at resonance $[U_{\mathrm{cr}}(=f_s h/S_t)]$, when shedding frequency $f_s = f'_a$, was estimated to be about 8.2 m/s, using a Strouhal number (S_t) of 0.22, as suggested by Welsh et al. [28] for similar w/h ratios. The distance between the trailing edge of the plate and the downstream wall of the cavities was about $9.8h$. This distance ensured an effective, resonant fluid-acoustic interaction in the near wake of the test model.

To generate the control perturbation, two cantilever actuators were simultaneously activated by a sinusoidal signal with controllable frequency, generated by a sine generator in the dSPACE control system, and then amplified by a dual-channel piezodriver amplifier (Trek PZD 700), as shown in Fig. 3. The acoustic pressures were measured by two 1/2 in. condenser microphones (B&K 4189). Microphone 1, referred to as mic. 1 hereafter, was flush-mounted on the top wall of the duct at $x = 23$ mm. Another microphone, mic. 2, was flush-mounted at the center of the top side wall of the cavity. A 5 μm tungsten single hot wire was deployed to measure the fluctuating flow velocity at various positions around the test model;

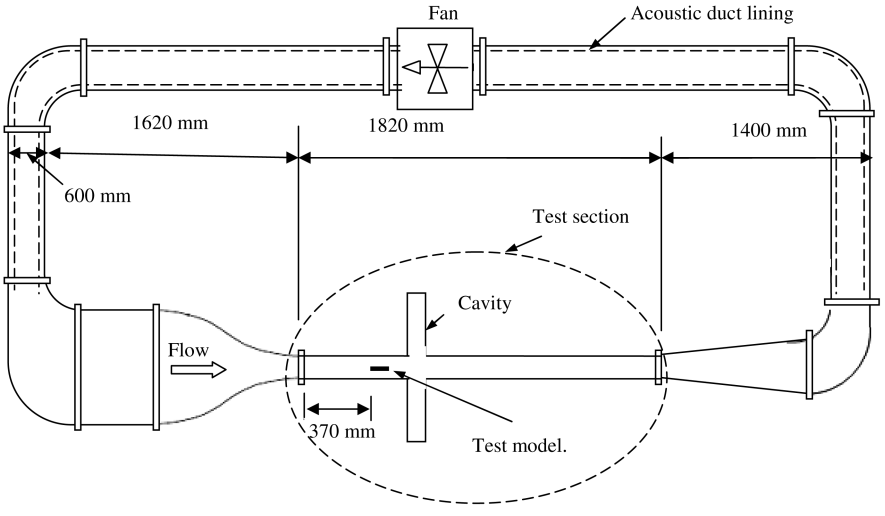

Fig. 1 Sketch of the wind-tunnel system.

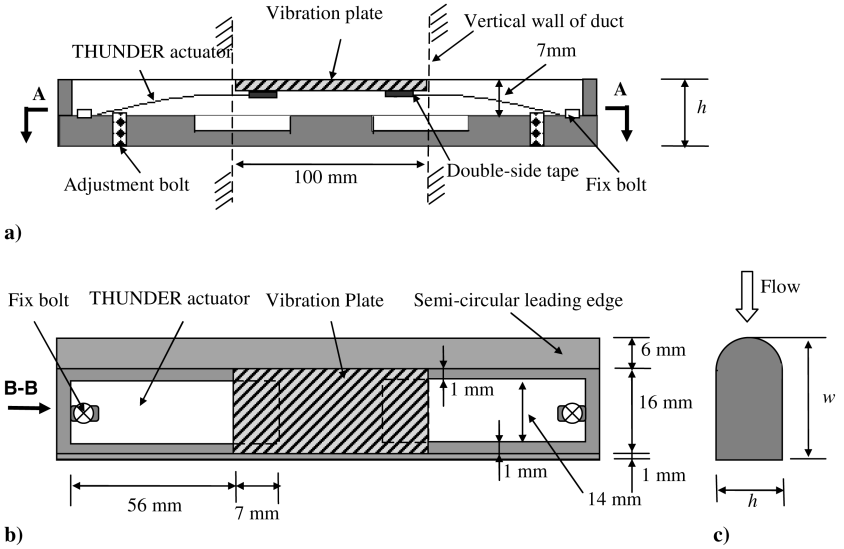

Fig. 2 The test model in detail: a) installation, b) top view A-A, and c) side view B-B.

these measured signals were amplified by using the Constant Temperature Anemometry (CTA) before being recorded into the computer. In addition, a Polytec Series 3000 dual-beam laser vibrometer was used to measure the perturbation displacement produced by the actuators. All measurement signals were recorded using a personal computer through a 12-bit analog-to-digital (AD) board at a sampling frequency of 6 kHz per channel after amplification. The duration of each record was about 11 s.

Before the installation of the test model, a single-boundary hot wire was used to measure the boundary-layer thickness (δ) at freestream flow velocity $U_\infty = 8.2$ m/s. The definition of δ is customarily the distance from the wall to the point where $u(y) = 0.99U_\infty$, beyond which the flow velocity is essentially U_∞. The measured δ was about 4.0 mm in the present case, corresponding to a uniform flow region in the duct from $y = -46$ mm to $y = 46$ mm in the y direction. The Reynolds number is 5980, based on the thickness of the bluff body and the freestream velocity $U_\infty = 8.2$ m/s. With a semicircular leading edge, the boundary layers on surfaces start to grow smoothly. In the present case, the boundary-layer growth is unlikely to be influenced by the inherent unsteadiness residing in flow because the turbulence intensity of the incoming flow is kept low (<0.1%). In addition, the test model has a relatively short chord, so the boundary-layer instability cannot be effectively developed. Therefore, the boundary layers remain attached over the surface of the test model up to the trailing edge.

III. Control Performance

Open-loop control tests were carried out at $U_\infty = 8.2$ m/s, corresponding to a shedding frequency $f_s = f'_a = 161.3$ Hz. The control performance was evaluated in the sound field (using mic. 1 at the trailing edge of the test model and mic. 2 inside the duct and flowfield simultaneously). The control frequency (f_p) and control voltage (V_p) of the controller were first determined. It was observed that best performance was obtained when $f_p = 30$ Hz with the highest permissible voltage of $V_p = 160$ V.

Figure 4 shows the sound pressure variation at the two microphone positions in the time domain before and after control. All time-

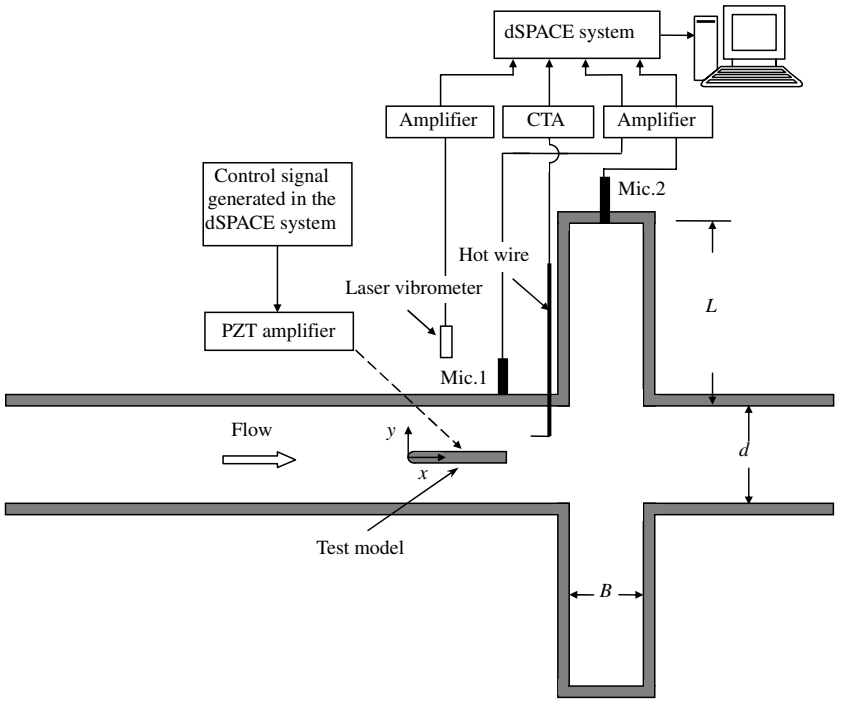

Fig. 3 Experimental setup, open-loop control system, and measurement system.

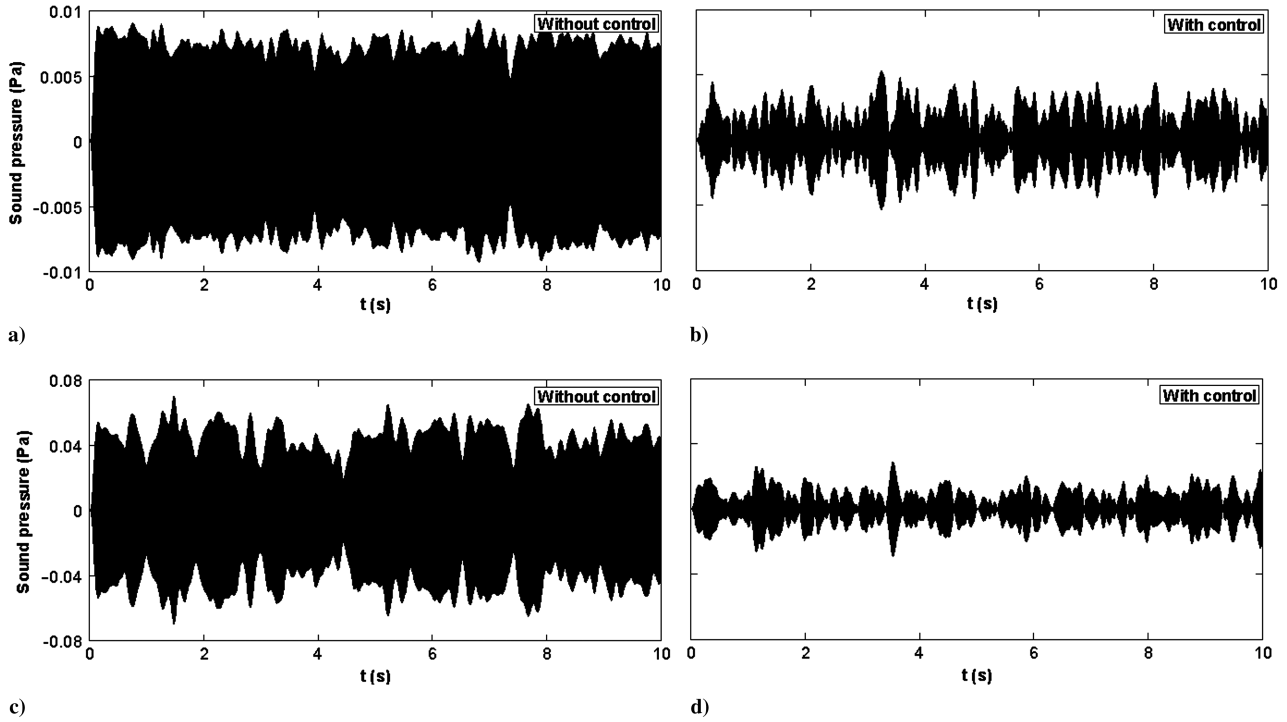

Fig. 4 Time-domain results for the control performance in sound field. a,b) Measured in the duct. c,d) Measured inside the cavity.

domain signals were filtered by a 5 Hz band around the shedding frequency. This allows for a better visualization of the signal change, relevant to the vortex shedding. It can be seen that, upon the deployment of the control, the sound pressure both in the duct and inside the cavity underwent significant reductions to different extents in the time domain. Noticing the difference in scale, the acoustic pressure is far more intense inside the cavity than it is in the duct, due to the resonance effect. The reduced level inside the cavity after the control also seems to be higher than that in the duct.

The control effect can be better assessed in the frequency domain. The spectra of the above time-domain signals were obtained using the Fast Fourier Transform (FFT) from the time-domain signals with a frequency resolution of 0.1 Hz. The fine resolution was needed for an accurate determination of the locations, as well as the values of the resonance peak corresponding to the shedding frequency. Results are shown in Fig. 5. It can be seen that, upon the deployment of the control, the SPL at mic. 1 decreases from 81.0 to 64.7 dB (a reduction of 16.3 dB) at the shedding frequency as shown in Fig. 5a. Meanwhile, mic. 2 recorded a decrease from 97.1 to 75.8 dB (a reduction of 21.3 dB), as shown in Fig. 5b, which was 5 dB larger than the reduction measured by mic. 1. In the meantime, higher-order harmonics of the resonance frequency also experienced reductions to different extents after the control. Judging from the higher reduction of the acoustic resonance inside the cavity, as compared to that in the duct, one can surmise that, in addition to the reduction in the vortex strength that serves as the source of the acoustic field, there should be other important physical phenomena involved during the control process. A careful examination of the dominant peak reveled that, in the present case, the shedding frequency was shifted from 161.3 to 158.4 Hz. This frequency-shift phenomenon, albeit not very obvious, as well as its impact on the acoustic resonance inside the cavity, will be further investigated in detail in the later part of this paper.

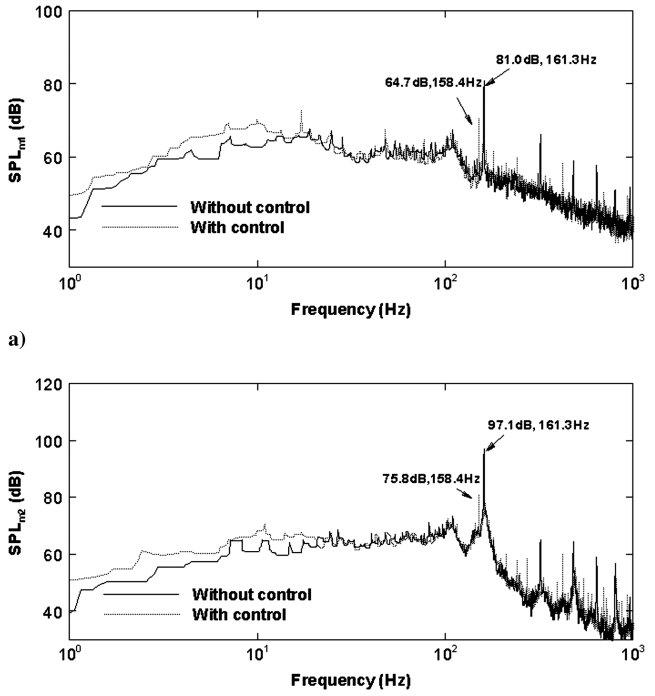

Fig. 5 Control performance of open-loop control in sound field: a) SPL measured by mic. 1, and b) SPL measured by mic. 2.

Corresponding changes in the flowfield, measured by hot wire at $x = 34$ mm and $y = 8.25$ mm, were examined in the time domain (Fig. 6) and in the frequency domain (Fig. 7), respectively. It can be seen that control has also successfully reduced the vortex strength, as evidenced by a significant reduction of the hot-wire signal in the time domain and the corresponding reduction in power-spectra density (E_u) at the shedding frequency. In fact, E_u decreases from 0.004107 to 0.000629, corresponding to a reduction of about 85%.

IV. Discussions on the Control Mechanisms

A. Vortex-Strength Abatement

1. Vortex Types and the Vortex-Structure Alteration

Measurements were performed to examine the vortex-shedding structure around the test model. While keeping one hot wire at the leading edge ($x = 0$ mm and $y = 11$ mm), referred to as hot wire 1, another hot wire was moved along x direction, keeping $y = 11$ mm, referred to as hot wire 2. The spectral phase $\phi_{u_1u_2}$ between the two hot wires showed the vortex distribution along the streamwise direction of the flow. The phase $\phi_{u_1u_2}$ was defined as $\phi_{u_1u_2} = \tan^{-1}$

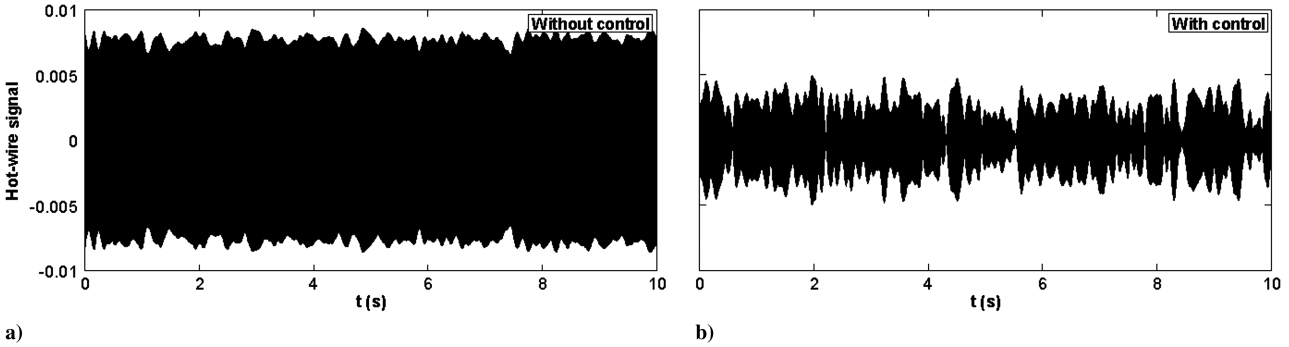

Fig. 6 Time-domain results for the control performance in sound field. a) Without control; b) With control.

$(Q_{u_1u_2}/Co_{u_1u_2})$, where $Co_{u_1u_2}$ and $Q_{u_1u_2}$ were the cospectrum and quadrature spectrum of u_1 and u_2, respectively. The cross-spectrum was computed from the fast Fourier transform of the correlation $\overline{u_1(t+\tau)u_2(t)}$. Measurement was first conducted without the test model to check the spectral phase $\phi_{u_1u_2}$ of the laminar boundary layer, resulting in $\phi_{u_1u_2} \approx 0$. The spectral phase $(\phi_{u_1u_2})$ was then measured before and after control, with results given in Fig. 8.

We focus first on the flow structure before control. The measurement of $\phi_{u_1u_2}$ was very close to zero within the semicircular leading-edge region $(x = 0 - 5.5$ mm) and started to fluctuate before the trailing edge ($x = 5.5 - 23$ mm). This implied that the laminar boundary layer in the vicinity of the leading edge was changed and redeveloped over the length of the test model, as evidenced by the regular change of $\phi_{u_1u_2}$ for the formation of vortex shedding after the trailing edge. In fact, when the vortex shedding was fully developed after the trailing edge and propagated further downstream, a clear trend of monotonically decreasing spectral-phase shifts was observed in the figure. Upon perturbing the test model's upper surface, the control brought about an obvious alteration to the flow structure. This alteration in $\phi_{u_1u_2}$ was rather irregular over the perturbed area (5.5 mm $< x <$ 25.5 mm), in which the boundary layer dominated. Further downstream, $\phi_{u_1u_2}$ was systematically increased as compared to its counterpart without control, implying that a longer time was required for a vortex to travel from the trailing edge to the downstream of the test model. This is consistent with the observation that the vortex-shedding frequency was reduced after control. Meanwhile, it indicated that the vortex-formation process had also been altered by the control action. This further impacted on the flow structure, as shown in Fig. 9, in which the nondimensional crossflow mean velocity $\bar{U}/U_\infty$ and root mean velocity values of Reynold stresses $\bar{u}^2/U_\infty^2$, $\bar{v}^2/U_\infty^2$ and $\overline{uv}/U_\infty^2$ behind the test model at $x = 34$ mm were measured and compared before and after control. Compared with the uncontrolled case, the extreme values of all four quantities were considerably reduced, ascribed to an impairment of the vortex strength and associated with a decreased entrainment of the flow. The observation also applies further downstream (not shown here), suggesting the persistency of the alteration. It is also relevant to notice that, although the perturbation was applied only on one side of the test model, effects seemed to be on both sides, as evidenced by the quasi-symmetrical/antisymmetrical feature of the curves shown in Fig. 9. This phenomenon can be explained by considering the formation mechanism of the vortex shedding. In fact, the vortex street is generated behind the test model through the interaction between the two separating shear layers on both sides of the bluff body. The one-sided perturbation disturbs one of the shear layers and subsequently alters its interaction with the other shear layer, leading to a reduction of the vortex-shedding strength.

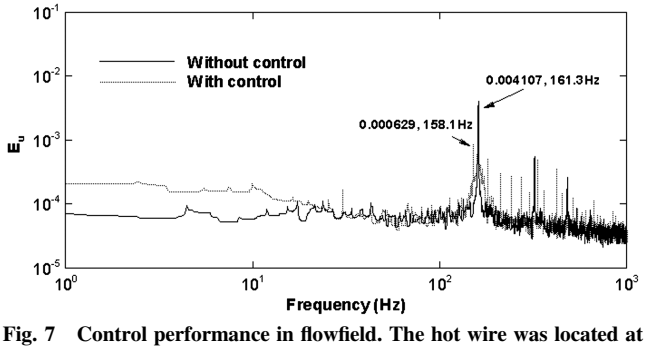

Fig. 7 Control performance in flowfield. The hot wire was located at $x = 34$ mm and $y = 8.25$ mm.

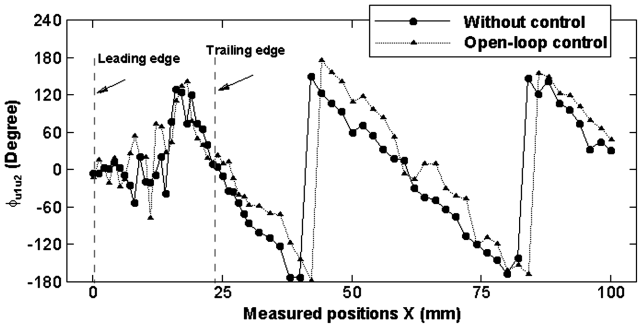

Fig. 8 Phase relationship between hot wire 1 and hot wire 2 along $y = 11$ mm.

2. *Control Mechanism*

Using the present system, measurements were carried out to deepen the understanding of the flow structure around the shedding frequency f_s. To this end, the peak values of E_{u_2} (the auto-spectrum of hot wire 2) at the vortex-shedding frequency f_s are shown in Fig. 10, before and after control. By focusing on the uncontrolled case, it can be seen that a peak in E_{u_2}, albeit very small (which can be verified by the E_{u_2} spectrum), exists even between the leading edge and the trailing edge. Because in the present configuration, with a semicircular leading edge, vortex shedding takes place after the trailing edge, the peak in E_{u_2} at the vortex-shedding frequency f_s measured by hot wire 2 before the trailing edge should come from a sort of hydrodynamic feedback from the trailing edge. This hydrodynamic feedback, referred to as a "pressure pulse," has been numerically revealed by Hourigan et al. [29]. Obviously, compared with the peak value in the strongest vortex-shedding region, the pressure pulse is indeed very small. Upon deployment of the open-loop control, the pressure pulse was reduced, as shown in Fig. 10. Considering the fact that the perturbation frequency was at 30 Hz and the peak value in E_{u_2} shown in Fig. 10 corresponded to the shedding frequency at 161.3 Hz, the observed reduction should be attributed to the effect of the pressure pulse.

Based on the above analysis, a complete interpretation of the control mechanism can be proposed. In the current configuration involving a test model with a semicircular leading edge, in which the incoming flow is rather uniform at a moderate Re, the boundary layer remains attached along the body of the test model and separates at the trailing edge. The free shear layers form each side of the body, then

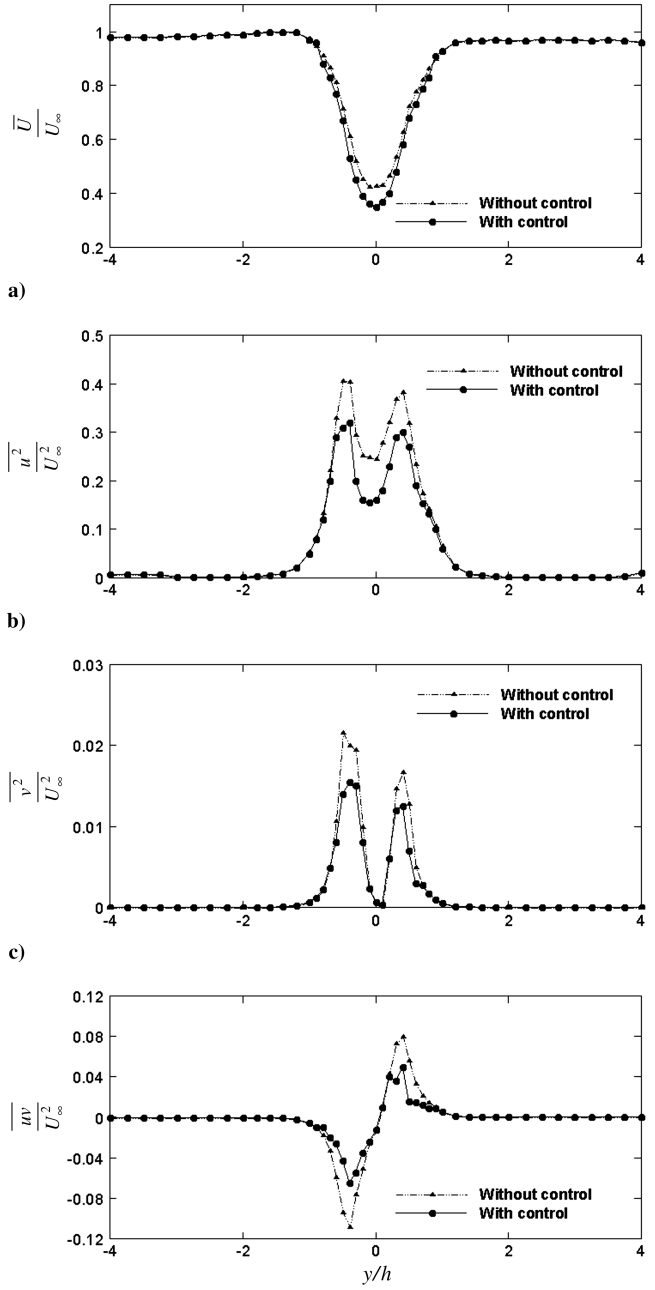

Fig. 9 Crossflow distribution of mean streamwise flow velocity and Reynolds stresses at y/h, open-loop control: a) $\bar{U}/U_\infty$, b) $\overline{u^2}/U_\infty^2$, c) $\overline{v^2}/U_\infty^2$, and d) $\overline{uv}/U_\infty^2$.

interact to form a vortex street after the trailing edge. Open-loop control causes additional vorticity that interacts with the vortex-shedding process to alter it. Further, additional vorticity from the oscillating plate will break up the spatial coherency of the trailing-edge vortex system, thus reducing its strength. Indeed, the oscillating plate would be expected to increase the mean boundary layer height at the trailing edge, thus reducing the shedding frequency, which will be demonstrated later in Sec. IV.B. Also contributing to this process might be the control-induced alteration in the hydrodynamic pressure pulse from the trailing edge. This translates into a perturbation in the boundary layer some distance upstream, due to the sudden flow oscillations caused by the trailing edge. In the present configuration, with a not-so-long chord length, this effect might go up to the leading edge, as shown in Fig. 10. Altogether, the perturbation alters the flow structure around the surface of the test model, which further disturbs the entrainment of the leading-edge boundary layer to the trailing edge and the feedback of the pressure pulse to the leading-edge

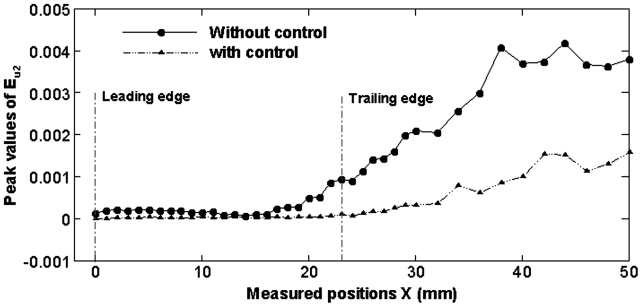

Fig. 10 The peaks of E_{u_2} measured by hot wire 2 between the leading edge and trailing edge.

boundary layer. This process alters the generation of trailing-edge vortex shedding, leading to a reduction of the vortex strength.

B. Frequency Shift and Its Impact on Acoustic Resonance

1. *Frequency-Shift Phenomenon*

Higher sound reduction inside the resonant cavity will be explained based on the shedding frequency-shift phenomenon. To that end, various measurements were conducted by varying the perturbation displacement of the vibration plate in the open-loop scheme. A corresponding shedding frequency (f_s) was obtained from the mic. 1 measurements. The displacement of the vibration plate (d_p) was measured by a laser vibrometer at the center point of the vibration plate. Results are shown in Fig. 11. It can be seen that the shedding frequency f_s was generally reduced upon deployment of the control. With a small perturbation amplitude of typically less than 0.4 mm, the reduction was trivial, typically less than 1 Hz. With a higher d_p, the reduction in f_s became more appreciable. In the optimum control configuration ($f_p = 30$ Hz and $V_p = 160$ V), with $d_p = 0.83$ mm, the shift in f_s could reach 2.84 Hz. The effect of this frequency shift on the control performance turns out to be very important, which will be assessed later.

The shift of the vortex-shedding frequency to lower frequencies can be attributed to the effect of the perturbation. Physically, the vortex-shedding frequency is determined by the distance between the two shear layers around the test model. Upon perturbation, the flow velocity generated by the vibration plate around the test model alters the thickness of the boundary layer around the test model, thus resulting in an increase in the distance between the two shear layers. This boundary-layer thickening results in a shift in the vortex-shedding frequency. Because it was difficult to accurately measure the boundary-layer thickening, we instead tried to quantify the frequency shift in terms of perturbation displacement, which is a piece of important information for people doing control. For that purpose, the effect of the perturbation can actually be loosely represented by an equivalent increase ($\bar{d}_p$) in the thickness of the test model (h). The perturbed shedding frequency (f_{sp}) can be expressed as

$$f_{sp} = \frac{S_t U_\infty}{h + \bar{d}_p} = \frac{S_t U_\infty}{h\left(1 + \frac{\bar{d}_p}{h}\right)} \tag{1}$$

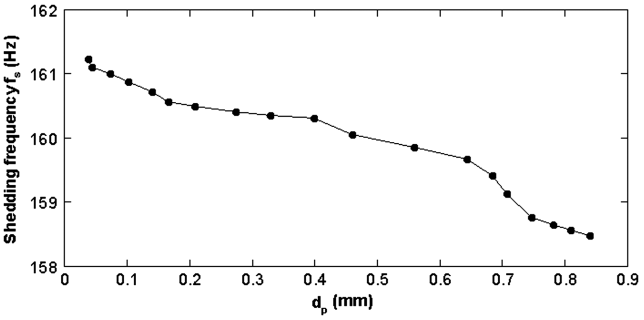

Fig. 11 Shift of shedding frequency at various maximum displacements d_p of the vibration plate, $f_p = 30$ Hz, measured by mic. 1.

Because h is much larger than $\bar{d}_p$, $\frac{\bar{d}_p}{h} \ll 1$ and

$$f_{sp} = \frac{S_t U_\infty}{h} \frac{1}{1+\frac{\bar{d}_p}{h}} \approx \frac{S_t U_\infty}{h}\left(1-\frac{\bar{d}_p}{h}\right) = f_{s0}\left(1-\frac{\bar{d}_p}{h}\right) \quad (2)$$

where f_{s0} is the unperturbed vortex-shedding frequency. The corresponding change (Δf_{sp}) can then be estimated by

$$\Delta f_{sp} = f_{s0} - f_{sp} = \frac{\bar{d}_p}{h} f_{s0} \quad (3)$$

Equation (3) shows that the reduction Δf_{sp} is linearly related to $\bar{d}_p$, which can be estimated by using the measured vortex-shedding frequency-shift data in Fig. 12 and Eq. (2). Figure 12 shows the variation of $\bar{d}_p$ versus d_p. The relationship between them can be best approximated using a linear regression fitting line, with a slope $\bar{d}_p/d_p = 0.2093$.

2. *Effect on Downstream Cavity Resonance*

The sound pressure level spectra measured by the two microphones are compared in Fig. 13 in terms of $\Delta\text{SPL} = \text{SPL}_{m2} - \text{SPL}_{m1}$, with SPL_{m2} and SPL_{m1} being the sound pressure levels at mic. 2 and mic. 1, respectively. In a region around the first cavity resonance frequency f'_a, the sound pressure level inside the cavity is obviously higher than that in the duct. This is clear evidence that sound is amplified by the cavity resonance effect. As an example, at resonance $f = f'_a$, the difference reached about 20 dB.

In order to explain the higher noise reduction inside the cavity as compared to that in the duct, the resonance bandwidth was determined. To this end, a series of tests were conducted to document the sound pressure levels measured by mic. 1 and mic. 2 at shedding frequency f_s under various flow velocities before the control was deployed. The results are shown in Fig. 14. The peak values of sound pressure level at f_s, measured by mic. 1, monotonously increase as the flow velocities increase. Its counterpart measured by mic. 2, however, reaches a peak value of 97.1 dB when $U_\infty = U_{\text{cr}} = 8.2$ m/s (i.e., $f_s = f = 161.3$ Hz). Using the conventional definition of the bandwidth corresponding to a 3 dB reduction compared to the peak value, the bandwidth of the resonance peak was determined as 3.4 Hz from 159.0 to 162.4 Hz, corresponding to a flow-velocity variation from 8.0 to 8.3 m/s.

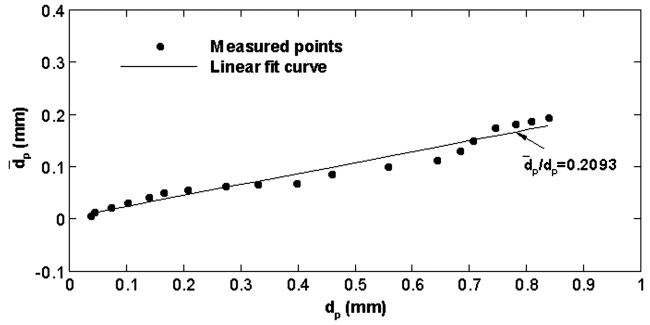

Fig. 12 The effective perturbation displacement of the vibration plate, $f_p = 30$ Hz.

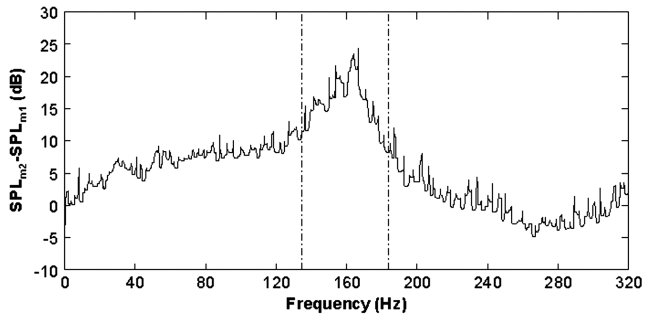

Fig. 13 Downstream cavity resonance, $L = 487$ mm, $d = 100$ mm, $U_\infty = 8.2$ m/s.

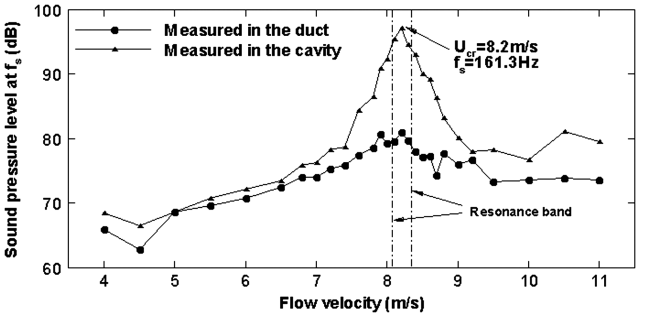

Fig. 14 Sound pressure level at f_s at various flow velocities, without control.

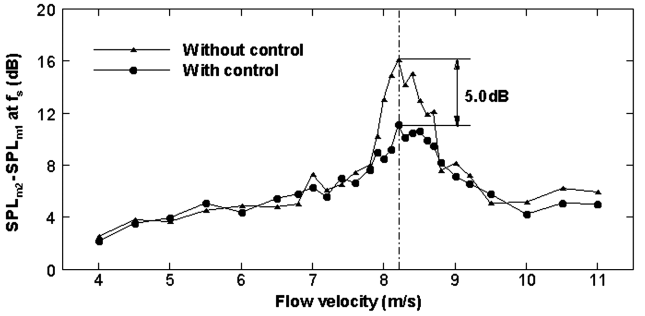

Fig. 15 Control effect on $\text{SPL}_{m2} - \text{SPL}_{m1}$ at f_s at various flow velocities, $f_p = 30$ Hz and $V_p = 160$ V.

Figure 15 shows the control effect on the previously defined ΔSPL at f_s at various flow velocities, with $f_p = 30$ Hz and $V_p = 160$ V. It can be seen that apart from the resonance region, the sound reduction in the duct and that in the cavity are almost the same. This should be attributed to the weakened vortex strength discussed in Sec. IV.A. Around the cavity resonance, however, the sound reduction inside the cavity exceeds that in the duct by as much as 5.0 dB. This can be attributed to the control-induced shift in the vortex-shedding frequency. In fact, a 2.84 Hz shift in f_s exceeds the half bandwidth of the cavity resonance; this alone should bring more than a 3 dB reduction in the SPL, which turned out to be 5 dB in the present case.

It now becomes clear that the successful control of the acoustic resonance inside the cavity is the fruit of a dual process: impairment of the vortex strength explained in Sec. IV.A and the offset of the acoustic resonance due to the shift in vortex-shedding frequency.

V. Conclusions

The control of flow-induced acoustic resonance has been experimentally investigated by using an active open-loop control system. The surface perturbation technique has been shown to be an effective way to suppress flow-induced acoustic resonance in an acoustic cavity downstream of a vortex generator. Meanwhile, a complete explanation of the control mechanism was achieved. Major conclusions can be summarized as follows:

1) Using an optimum control configuration, the SPL at the vortex-shedding frequency was reduced by 16.3 dB in the duct and 21.3 dB inside the cavity. This control performance was found to be repeatable and reliable.

2) The reduction of flow-induced noise in the duct is mainly due to the impairment of the vortex strength upon deployment of the control. It is proposed that the local perturbation alters the flow structure around the surface of the test model, which further disturbs the entrainment of the leading-edge boundary layer to the trailing edge. Further, additional vorticity from the vibration plate breaks up the spatial coherency of the trailing-edge vortex system, thus

reducing its strength. By the same token, the feedback of the pressure pulse to the leading-edge boundary layer is also affected, adding its contribution to the impairment of the vortex-shedding strength.

3) In addition, the local surface perturbation brought about a shift in the shedding frequency, which can be roughly estimated using a formula derived from experimental measurement. This frequency shift, albeit slight, may result in an offset of the acoustic resonance beyond its resonance bandwidth, especially for a lightly damped acoustic cavity. This phenomenon alone results in additional sound reduction inside the cavity, as evidenced by the higher sound reduction inside the cavity as compared to that obtained in the duct.

4) Based on the experimental data, an empirical formula was derived to predict this vortex-shedding frequency shift in the effective control region. In the present case, the control resulted in a 1.7% increase in the effective height of the test sample, leading to a frequency shift of about 2.84 Hz, responsible for a further sound pressure reduction of 5 dB inside the acoustic cavity.

Acknowledgments

The authors wish to acknowledge support given to them by the Research Grants Council of Hong Kong Special Administrative Region (HKSAR) through Grant No. PolyU 5132/07E. Appreciations also go to Randolph C. K. Leung for his useful input in finalizing the paper.

References

[1] Gerrard, J. H., "The Mechanics of the Formation Region of Vortices Behind Bluff Bodies," *Journal of Fluid and Mechanics*, Vol. 25, No. 2, 1966, pp. 401–413. doi:10.1017/S0022112066001721

[2] Nakamura, Y., Ohya, Y., and Tsuruta, H., "Experiments on Vortex Shedding from Flat Plates with Square Leading and Trailing Edges," *Journal of Fluid and Mechanics*, Vol. 222, Jan. 1991, pp. 437–447. doi:10.1017/S0022112091001167

[3] Nakayama, R., Nakamura, Y., Ohya, Y., and Ozono, S., "A Numerical Study of the Flow Around Flat Plates at Low Reynolds Numbers," *Journal of Wind and Industrial Aerodynamics Engineering*, Vols. 46–47, Aug. 1993, pp. 255–264. doi:10.1016/0167-6105(93)90291-U

[4] Cattafesta, L., Williams, D., Rowley, C., and Alvi, F., "Review of Active Control of Flow-Induced Cavity Resonance," AIAA Paper 2003-3567, 2003.

[5] Shih, W. C. L., Wang, C., Coles, D., and Roshko, A., "Experiments on Flow Past Rough Circular Cylinders at Large Reynolds Numbers," *Journal of Wind and Industrial Aerodynamics Engineering*, Vol. 49, Nos. 1–3, 1993, pp. 351–368. doi:10.1016/0167-6105(93)90030-R

[6] Anderson, E., and Szewczyk, A., "Effects of a Splitter Plate on the Near Wake of a Circular Cylinder in 2 and 3-Dimensional Flow Configurations," *Experiments in Fluids*, Vol. 23, No. 2, 1997, pp. 161–174. doi:10.1007/s003480050098

[7] Sukri, M., Ali1, M., Doolan, C. J., and Wheatley, V., "Low Reynolds Number Flow over a Square Cylinder with a Splitter Plate," *Physics of Fluids*, Vol. 23, No. 3, 2011, pp. 1–12. doi:10.1063/1.3563619

[8] Dehkordi, B. G., and Jafari, H. H., "On the Suppression of Vortex Shedding from Circular Cylinders Using Detached Short Splitter-Plates," *Journal of Fluids Engineering*, Vol. 132, No. 4, 2010, p. 044501. doi:10.1115/1.4001384

[9] Doolan, C. J., "The Interaction of a Flat Plate with the Near Wake of a Square Cylinder," *AIAA Journal*, Vol. 47, No. 2, 2009, pp. 475–479. doi:10.2514/1.40503

[10] Dalton, C., Xu, Y., and Owen, J. C., "The Suppression of Lift on a Circular Cylinder Due to Vortex Shedding at Moderate Reynolds Numbers," *Journal of Fluids and Structures*, Vol. 15, Nos. 3–4, 2001, pp. 617–628. doi:10.1006/jfls.2000.0361

[11] Baek, S., and Sung, H. J., "Numerical Simulation of the Flow Behind a Rotary Oscillating Circular Cylinder," *Physics of Fluids*, Vol. 10, No. 4, 1998, pp. 869–876. doi:10.1063/1.869610

[12] Choi, S., Choi, H., and Kang, S., "Characteristics of Flow over a Rotationally Oscillating Cylinder at Low Reynolds Number," *Physics of Fluids*, Vol. 14, No. 8, 2002, pp. 2767–2777. doi:10.1063/1.1491251

[13] Cetiner, O., and Rockwell, D., "Streamwise Oscillations of a Cylinder in a Steady Current. Part 1: Locked-On States of Vortex Formation and Loading," *Journal of Fluid and Mechanics*, Vol. 427, 2001, pp. 1–28. doi:10.1017/S0022112000002214

[14] Blackburn, H., and Henderson, R., "A Study of Two-Dimensional Flow Past an Oscillating Cylinder," *Journal of Fluid and Mechanics*, Vol. 385, 1999, pp. 255–286. doi:10.1017/S0022112099004309

[15] Berger, E., "Suppression of Vortex Shedding and Turbulence Behind Oscillating Cylinders," *Physics of Fluids*, Vol. 10, No. 9, 1967, pp. 191–193. doi:10.1063/1.1762444

[16] Huang, X. Y., and Weaver, D. S., "On the Active Control of Shear Layer Oscillations Across a Cavity in the Presence of Pipeline Acoustic Resonance," *Journal of Fluids and Structures*, Vol. 5, No. 2, 1991, pp. 207–219. doi:10.1016/0889-9746(91)90472-2

[17] Cattafesta, L. N., III, Garg, S., Choudhari, M., and Li, F., "Active Control of Flow-Induced Cavity Resonance," AIAA Paper 1997-1804, 1997.

[18] Cattafesta, L. N., III, Garg, S., and Shukla, D., "The Development of Piezoelectric Actuators for Active Flow Control," *AIAA Journal*, Vol. 39, No. 8, 2001, pp. 1562–1568. doi:10.2514/2.1481

[19] Cattafesta, L. N., III, Mathew, J., and Kurdila, A., "Modeling and Design of Piezoelectric Actuators for Fluid Flow Control," *SAE 2000 Transactions Journal of Aerospace*, Vol. 109, 2001, pp. 1088–1095. doi:10.4271/2000-01-5534

[20] Cheng, L., Zhou, Y., and Zhang, M. M., "Perturbed Interaction Between Vortex Shedding and Induced Vibration," *Journal of Fluids and Structures*, Vol. 17, No. 7, 2003, pp. 887–901. doi:10.1016/S0889-9746(03)00042-2

[21] Marouzé, J. P., and Cheng, L., "A Feasibility Study of Active Vibration Isolation THUNDER Actuators," *Smart Materials and Structures*, Vol. 11, No. 6, 2002, pp. 854–862. doi:10.1088/0964-1726/11/6/305

[22] Zhang, M. M., Cheng, L., and Zhou, Y., "Closed-Loop-Controlled Vortex Shedding from a Flexibly Supported Square Cylinder Under Different Schemes," *Physics of Fluids*, Vol. 16, No. 5, 2004, pp. 1439–1448. doi:10.1063/1.1687413

[23] Cheng, L., Zhou, Y., and Zhang, M. M., "Controlled Flow-Induced Vibration on a Fix-Supported Flexible Cylinder in Crossflow," *Journal of Sound and Vibration*, Vol. 292, Nos. 1–2, 2006, pp. 279–299. doi:10.1016/j.jsv.2005.07.044

[24] Zhang, M. M., Cheng, L., and Zhou, Y., "Closed-Loop Controlled Vortex-Airfoil Interactions," *Physics of Fluids*, Vol. 18, No. 4, 2006, p. 046102. doi:10.1063/1.2189287

[25] Zhang, M. M., Cheng, L., and Zhou, Y., "Control of Post-Stall Airfoil Aerodynamics Based on Surface Perturbation," *AIAA Journal*, Vol. 46, No. 10, 2008, pp. 2510–2519. doi:10.2514/1.35792

[26] Zhang, M. M., Cheng, L., and Zhou, Y., "Asynchronous Control of Flow-Induced Acoustic Cavity Resonance Using Imbedded Piezo-Electric Actuators," *Journal of Acoustical Society of America*, Vol. 126, No. 1, 2009, pp. 36–45. doi:10.1121/1.3143784

[27] Ziada, S., and Shine, S., "Strouhal Numbers of Flow-Excited Acoustic Resonance of Closed Side Branches," *Journal of Fluids and Structures*, Vol. 13, No. 1, 1999, pp. 127–142. doi:10.1006/jfls.1998.0189

[28] Welsh, M. C., Stokes, A. N., and Parker, R., "Flow-Resonant Sound Interaction in a Duct Containing a Plate, Part I: Semi-Circular Leading Edge," *Journal of Sound and Vibration*, Vol. 95, No. 3, 1984, pp. 305–323. doi:10.1016/0022-460X(84)90670-9

[29] Hourigan, H., Thompson, M. C., and Tan, B. T., "Self-Sustained Oscillations in Flows Around Long Blunt Plates," *Journal of Fluids and Structures*, Vol. 15, Nos. 3–4, 2001, pp. 387–398. doi:10.1006/jfls.2000.0352

M. Glauser
Associate Editor